E4-2001-75

V.K.Lukyanov, V.P.Permyakov, Yu.V.Chubov

DESCRIPTION OF ELASTIC SCATTERING OF HEAVY IONS IN THE GLAUBER–SITENKO APPROACH

Submitted to «Ядерная физика»

1 Introduction

The nature of scattering of heavy ions by nuclei depends, to a great extent, on the specificity of the behavior of a potential on its periphery where an essential role is played by a powerful but slightly changing Coulomb potential, and on the contrary, a sharply changing nuclear potential. In this case, it is important to employ extended optical potentials of the Woods–Saxon type with a large range of interaction. Note is to be made that, at present, there are effective calculations programs for the scattering differential cross section. However, it is better to consider the problems concerning the physical picture of the process on the basis of analytic methods of calculation and analysis of the corresponding amplitudes. They allow one, for instance, to understand why the nature of angular distributions changes with growing scattering angles, how they depend on the energy and set of colliding nuclei, what can be expected if either parameters of the problem are varied. Approaches of that sort were developed for diffraction scattering models where experimental data are fitted through matching parameters of either form if the scattering S-matrix given phenomenologically (see, e.g., [1–4]). The physical language taken from the optical interference and diffraction was adapted for interpreting the angular distributions of elastic scattering of nuclei.

In recent years, in the heavy-ion scattering problems, wide use has been made both of phenomenological nucleus–nuclear potentials and microscopic potentials constructed by using effective NN-forces and the nuclear density distribution functions, an account was taken of the exchange effects and the density dependence of forces, and so on [5–8]. This creates a more profound physical basis of understanding the scattering mechanism itself and manifestation of peculiarities of the nucleus structure, for instance, of the neutron or proton halo on a remote periphery of some light nuclei, neutron excess in the surface region of nuclei, the influence of the nuclear-matter compression on internuclear forces. In this connection, it seems of interest to develop the analytic methods of calculation of amplitudes within the framework of the potential approach. In this case, the problem is not only to qualitatively consider the scattering picture, but also to make quantitative computations that reproduce exact numerical solutions at the same given potential.

In the paper, heavy-ion scattering is considered at energies from 10 to 100 MeV/nucleon when the condition $E \gg V$ is justified, and the wavelength is small as compared to the characteristic parameters: radius R and thickness a of the surface layer of the potential. (Here E is the collision energy; V, the interaction potential). Then, one can take the Glauber–Sitenko approach [9,10] as the basis, in which the eikonal amplitude is obtained in closed form for small scattering angles $\vartheta < \sqrt{2/kR}$ (k is the collision momentum). This approach is widely used in hadron–nucleus scattering where the Gaussian shape of a potential or the density of a target–nucleus is usually employed. Then integration in the phase that proceeds along the straight trajectory of motion can be performed explicitly,

and in some cases, the amplitude can be obtained in a certain form. Unfortunately, it is just this form of the approach that cannot be applied to heavy–ion scattering. The specific feature of the latter is that it should be modified to take account, first, of the strong Coulomb distortion of the trajectory of motion. Now, this latter deviates off the straight line along the initial momentum $\vec{k}_i$ on the deflection angle $\theta_c \simeq Z_1 Z_2 e^2/RE$, where R is the sum of radii of colliding nuclei. The other specific point is the always large radius of interaction which arrive at a conclusion to employ extended forms of potentials of the Saxon–Woods type that strongly differ from Gaussian potentials. For those potentials, the eikonal phase was not yet found in an explicit form; and this made it impossible to develop analytic methods of evaluation of the nucleus–nuclear amplitude. And only recently in ref.[11], its approximate expression was obtained for a symmetrized Saxon–Woods potential. It rather accurately reproduces the behavior of the exact numerical phase and thus allows one to determine the differential cross section coincident with exact calculations. And this, in turn, made it possible to adapt the known asymptotic methods of estimation of rapidly oscillating integrals to the problem of nucleus–nucleus scattering and its specific character.

In this paper, we derived the amplitudes in explicit form corresponding to their typical regimes of scattering in certain angular intervals. Effects of deviation of the motion trajectory connected with the influence of the strong Coulomb field are discussed and taken into account. As a result, the range of angles could be increased where the Glauber–Sitenko approach is valid. The accuracy of analytic calculations was controlled by numerical computations of angular distributions, and comparison with experimental data was carried out.

2 The Method

The scattering amplitude in the Glauber–Sitenko approach is of the form [9, 10]:

$$f(q) = -ik \int_0^\infty J_0(qb) \Big[e^{i\chi(b)} - 1 \Big] b \, db. \tag{1}$$

Here $q = 2k \sin(\vartheta/2)$ is the momentum transferred; ϑ is the scattering angle; the eikonal phase is given by

$$\chi(b) = -\frac{k}{2E} \int_{-\infty}^{\infty} V(\sqrt{b^2 + z^2}) \, dz, \tag{2}$$

and b is the impact parameter. The interaction potential consists of the nuclear and Coulomb parts:

$$V(r) = V_N(r) + V_C(r). \tag{3}$$

The nuclear potential is usually taken to be the optical Woods–Saxon potential

$$V_N(r) = (V_0 + iW_0)u_F(r), \qquad u_F(r) = \left(1 + \exp\frac{r-R}{a}\right)^{-1}, \tag{4}$$

whereas the Coulomb potential is chosen in the traditional form

$$V_C(r) = \frac{V_B}{2}\left(3 - \frac{r^2}{R_C^2}\right)\Theta(R_C - r) + \frac{V_B}{r}R_C\,\Theta(r - R_C), \quad V_B = \frac{Z_1 Z_2 e^2}{R_C}, \tag{5}$$

which corresponds to the interaction of change $Z_1 e$ with a uniformly distributed charge $Z_2 e$ in the sphere of radius R_C.

Owing to the condition $kb \gg 1$, the integral in the amplitude (1) oscillates strongly. This makes it possible to use the asymptotic methods for its estimation. The Bessel function is replaced by its asymptotic expression $J_0(x) = \sqrt{2/\pi x}\,\cos(x - \pi/4)$, $(x \gg 1)$; besides, in (1), when scattering proceeds through angles $\vartheta \neq 0$, it suffices to consider only the first term. Then we obtain

$$f(q) = f_{(+)} - f_{(-)}, \qquad f_{(\pm)} = -\frac{1}{4\sin(\vartheta/2)}\sqrt{\frac{q}{\pi}}\,(1 \pm i)\,t_{(\pm)}, \tag{6}$$

$$t_{(\pm)} = \int_0^\infty \sqrt{b}\,db\,e^{ig_{(\pm)}(b)}, \tag{7}$$

$$g_{(\pm)}(b) = \pm qb + \chi(b), \qquad \chi(b) = \chi_N(b) + \chi_C(b). \tag{8}$$

Here $\chi_N(b)$ and $\chi_C(b)$ are the nuclear Coulomb phases calculated by eq.(2) with the appropriate potentials (4) and (5). The $f_{(-)}$ and $f_{(+)}$ are called the near-side and far-side amplitudes; in the quasiclassical limit, they are associated with the trajectories of deflection around the near and remote edges of a scatterer.

The methods of evaluations of integrals with rapidly oscillating functions such as the pole method, the steepest descents and stationary phase methods, require the assumed phases $\chi(b)$ in an explicit analytic form. Note that the phases $\chi(b)$ defined by (2) are integrals of the potential along the straight trajectory of motion of nuclei. For the Coulomb potential, this phase is calculated explicitly [12]:

$$\chi_C(b) = \frac{\eta}{R_C}\left\{\left[-\frac{8}{3}\,\xi + \frac{2b^2}{3R_C^2}\,\xi + 2R_C\ln(k(R_C + \xi))\right]\Theta(R_C - b) + \right.$$
$$\left. +2R_C\ln(kb)\,\Theta(b - R_C)\right\}. \tag{9}$$

Here $\xi = \sqrt{R_C^2 - b^2}$, and $\eta = Z_1 Z_2 e^2 k/2E$ is the Sommerfeld parameter. For the nuclear potential in the form of the Saxon–Woods potential (4) no analytic expression can be obtained for the phase χ_N. To overcome this difficulty, approaches were developed, in which that potential or the phase $\chi_N(b)$ were simulated by the sum of Gaussian functions,

whose weight coefficients as well as the parameters of the functions were adjusted with a sufficient accuracy [13, 14]. Here every time for a new set of parameters of the Woods–Saxon potential, one should repeat the procedure of fitting. Besides, in view of the mentioned specificity of nucleus-nucleus scattering, it is highly important to use a more realistic exponential asymptotics than the Gaussian asymptotics for the potential in the region of its periphery.

In ref. [11], another method was proposed based on an approximate separation of variables b and z in the integrand of (2). Moreover, a more realistic symmetrized Fermi function was taken as the distribution function of the potential

$$u_{SF}(r) = \frac{\sinh\ C}{\cosh\ C + \cosh\ r/a}, \qquad C = R/a, \tag{10}$$

that coincides with $u_F(r)$ in the region $r > 0$ when $R \gg a$. The potential with the u_{SF} distribution has the correct behavior in the center, namely, its derivative $u'_{SF}(0) = 0$, while the traditional Woods–Saxon potential has the divergence at the center which differs from zero ($u'_F(0) \neq 0$). Thus, hereafter it is more appropriate to employ the symmetrized Woods–Saxon potential [15]. Moreover, as it has been shown in [11], for this potential one can derive an approximate analytic expression for the nuclear phase:

$$\chi_N(b) = -kR\frac{V_0 + iW_0}{E}\ P(1, C)\ u_{SF}(b), \tag{11}$$

where

$$P(1, C) = \frac{1}{C}\ [2.489453 + 0.34597\ C - 0.0046\ C^2].$$

In the region of the potential periphery $b \sim R$, it well reproduces the phase obtained by numerical integration (2). What is more, it has been verified [11] that the corresponding differential cross sections of elastic scattering, calculated with the phase found numerically and the phase (11), coincide with a good accuracy in the whole range of applicability of the Glauber–Sitenko approach.

In what follows, we develop the approximate methods for calculating the amplitudes on the basis of analytic expressions of phases (9) and (11). In our case of nucleus–nucleus scattering, we have $qb \simeq qR \gg 1$, which allows us to employ the asymptotic method of stationary phase. According to this method, the exponent $g_{(\pm)}$ in (7) should be expanded in the Taylor series in the vicinity of saddle points b_{s_n} that determine regions of a major contribution to the integral. So, we write

$$g_{(\pm)}(b) = g_{(\pm)}(b_{s_n}) + g'_{(\pm)}(b_{s_n})\ (b - b_{s_n}) + \frac{g''_{(\pm)}(b_{s_n})}{2}\ (b - b_{s_n})^2 + ..., \tag{12}$$

and, from the condition for the first derivative being equal to zero, we derive the equation for stationary points (saddle points):

$$\pm\, q + \chi'_N(b_{s_n}) + \chi'_C(b_{s_n}) = 0. \tag{13}$$

Consider the case when $W_0 = 0$ [1] Then equation (13) will contain real quantities, and its solutions produce the dependence $q = q(b)$. For the reaction of nucleus–nucleus scattering usually considered, it turns out that a stationary point, a solution to the equation for $g_{(+)}$, lies outside of the range of integration. Therefore the term $f_{(+)}$ can be neglected in (6), and the scattering amplitude $f(q)$ is determined only by the near-side amplitude $f_{(-)}$. For the heavy ion scattering, a situation is typical when the equation for $g_{(-)}$ gives two solutions, and thus, two saddle points b_{s_1} and b_{s_2} give a leading contribution to the amplitude. If they are situated sufficiently far from each other [2], their contributions can be considered as independent, and the near amplitude $f_{(-)}$ is determined by the sum of contributions from vicinities of those points. Now, we insert (12) with $g'_{(\pm)}(b_{s_n}) = 0$ into the integral (7), take the slowly changing factor $\sqrt{b}$ out of the integral sign, and tend the limits of integration to the right and to the left from b_{s_n} to infinity. Then the integral is calculated explicitly, and the amplitude takes the form

$$f_{(-)} = -\frac{1}{4\sin(\vartheta/2)}\sqrt{\frac{q}{\pi}}\,(1-i)\sum_{n=1,2} t_{(-),n}, \tag{14}$$

where

$$t_{(-),n} = \sqrt{b_{s_n}}\sqrt{\frac{2\pi}{g''_{(-)}(b_{s_n})}}\; e^{i(g_{(-)}(b_{s_n})+\pi/4)}. \tag{15}$$

In Fig. 1, we show the dependence $q = q(b)$ for scattering of ^{17}O on ^{208}Pb at energy $E_{c.m.} = 1327$ МэВ. The dot–dashed curve is the curve of stationary points for the Coulomb scattering phase $\chi_C = 2\eta\ln(kb)$ in the field of two point charges Z_1e and Z_2e, whereas the point line to the left of the top shows a small deviation that arises if the point charge Z_1e is scattered in the field (5) of the uniformly distributed charge Z_2e in the sphere of radius R_C. The solid curve is the numerical solution to equation (13) with the phase χ_N determined by expressions (11) and the Coulomb phase $\chi_C = 2\eta\ln(kb)$, while the long-dashed curve shows the solution when in equation (13) χ_C is changed by the exact Coulomb phase (9). It is seen, that throughout the whole periphery region of the nucleus–nucleus potential, the solid and long-dashed curves coincide very closely. Therefore, instead of the total Coulomb phase (9), one can use only its asymptotic part $2\eta\ln(kb)$. For Fig. 1 it is seen that the deviation function $q(b)$ has a typical maximum $q_{max} \equiv q_r = q(b_r)$ in the region of interaction surface that determines the basic features of the scattering picture. In this region of the limiting classical momentum transfer, it is convenient to represent the

[1] In final expressions, we replace V_0 by $V_0 + iW_0$, which is valid for $W_0 \ll V_0$. In the periphery region when $b \sim R_1 + R_2$ and at classical scattering angles $\vartheta < |V|/E$, this results in a minor renormalization of the particle flux by factor $(1 - W_0/4E)$ (see, for instance, [16]). In a more general case for complex variables, the method of stationary phase was developed in ref. [17] for the diffraction model of scattering.

[2] The given points are saddle points of the first order, since $g''_{(-)}(b_{s_n}) \neq 0$.

function $q(b)$ at the logarithmic parabola [18]

$$q = q_r - \rho\left\{\ln\frac{b-b_1}{b_r-b_1}\right\}^2, \tag{16}$$

where parameters b_r, q_r, b_1, ρ are determined from fitting this parabola to the exact curve $q(b)$ obtained by numerical solution of equation (13) for the stationary point.

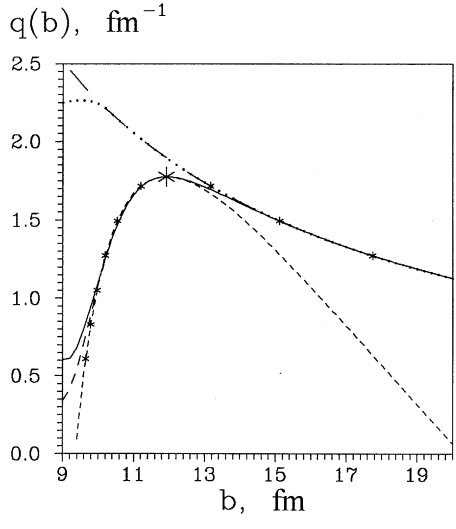

Рис 1: *Dependence of the deviation function on the impact parameter constructed on the basis of the eikonal phase for scattering of* $^{17}O+\ ^{208}Pb$ *(*$E_{c.m} = 1327$ *MeV). The potential parameters are reported in Table 1, and the eikonal phases are defined by (9) and (11).*

As it turns out, for a typical combination of the Coulomb and nuclear potentials characteristic of the nucleus–nucleus scattering, a fit like that should be accomplished as accurated as possible. Specifically, methodical computations show that, if the position of b_r is determined with an accuracy of an order of 0.5 fm, the cross section is changed by an order of magnitude. Besides, our aim was also to obtain the explicit dependence of parameters of this logarithmic parabola on input parameters of the problem, namely, on geometric parameters and power parameters of given potentials. For this purpose, a particular method was developed, according to which the first derivative of the function $q(b)$ in the region of its maximum was first approximated by a polynomial of the third degree, and then an equation was derived that gave solutions for b_r, q_r, b_1, ρ in an explicit form (see Appendix A). In this way, the parabola (16) was completely determined, and then it was used to derive two solutions for saddle points:

$$\begin{aligned} b_{s_1} &= b_1 + (b_r - b_1)\exp\{-\sqrt{(q_r-q)/\rho}\}, \\ b_{s_2} &= b_1 + (b_r - b_1)\exp\{+\sqrt{(q_r-q)/\rho}\}. \end{aligned} \tag{17}$$

This approximation of the function $q(b)$ in the region of its maximum by the logarithmic parabola is shown in Fig. 1 with a fine dashed line. Note that b_1 in formula (16) is a point of intersection of the curve of momentum deviation $q(b)$ with the axis b from the left, whereas b_r and q_r show the point (a large asterisk in Fig. 1) of the classical momentum boundary $q \leq q_r$ of applicability of a classical scattering theory. From this figure it is seen that the logarithmic parabola well reproduces the vertex and the left part of the deviation function where the saddle points b_{s_1} are situated. To the right, the dependence $q(b)$ is determined by the first derivative of the asymptotic part of the Coulomb phase (9), and it is described by the saddle points $2\eta/q$. So, the behaviors of the deviation function is determined by the following set of saddle points

$$\begin{aligned} b_{s_1} &= b_1 + (b_r - b_1)\exp\{-\sqrt{(q_r - q)/\rho}\}\ , \quad b < b_r \\ b_{s_2} &= 2\eta/q \qquad\qquad\qquad\quad , \quad b > b_r. \end{aligned} \tag{18}$$

These points are shown in Fig. 1 by asterisks.

3 Classical and quantum scattering regions

At angles $\vartheta < \vartheta_r$ ($q < q_r$), scattering proceeds in the classical region; at every angle ϑ, there are two trajectories of motion with different impact parameters b_{s_1} and b_{s_2}.

Numerical and analytic calculations of the ratio of the elastic scattering cross section to the Rutherford cross section $d\sigma/d\sigma_R$ are presented in Fig. 2 [3]. The amplitude $f(q)$ is defined by eqs. (6) and (15). The absorption is taken into account via changing the real potential by the complex one in the final expression for the amplitude. It is seen that the analytic calculations are in good agreement with the numerical computations, except for the region of angles close to ϑ_r, which corresponds to the extremum of the deviation function $q(b)$. At $\vartheta = \vartheta_r$, the cross section becomes infinite, since the second derivative $g''_{(-)}(b_r)$ in the denominator of (15) turns into zero.

When $\vartheta < \vartheta_r$ $(q < q_r)$ the ratio of cross sections $d\sigma/d\sigma_R$ oscillates with respect to unity. This occurs due to interference between the nuclear and Coulomb amplitudes determined by different saddle points b_{s_1} and b_{s_2} from (18) and having, respectively, different phases $g_{(-)}(b_{s_1})$ and $g_{(-)}(b_{s_2})$. As a result, the absolute value of the amplitude squared

$$|f(q)|^2 = |f[b_{s_1}(q)]|^2 + |f[b_{s_2}(q)]|^2 + \\ + \frac{2k^2}{q^2}\sqrt{\frac{q\pi b_{s_1} b_{s_2}}{g''_{(-)}(b_{s_1})g''_{(-)}(b_{s_2})}}\ \cos[g_{(-)}(b_{s_1}) - g_{(-)}(b_{s_2}].$$

contains a nonzero interference term. The nuclear amplitude $f[b_{s_1}(q)]$ at small angles $\vartheta < \vartheta_r \simeq |V|/E$ is always small as compared to the Coulomb amplitude, and thus, it

[3] In these and further calculations, account is taken of the Coulomb distortion of the straight trajectory of motion, i.e. the path of integration in eq.(2). These effects will be discussed in section 6.

manifests itself as interference. When $\vartheta \to 0$, oscillations are completely suppressed by the Rutherford scattering. When absorption is included, $W_0 \neq 0$, the flux of particle in the elastic channel diminishes, which smoothers oscillations. This scattering picture corresponds to the Fresnel diffraction in optics that results from interference between an incident beam and a beam scattered at the edge of a screen.

As the saddle points b_{s_1} and b_{s_2} approach the limit point of maximum (at b_r), regions near each of them which give main contributions to the amplitude, start to overlap. In this case, the estimate (15) of the integrals and the assumption of their independent contribution to the amplitude lose their meaning. The problem can be resolved either by the addition of subsequent expansion terms of the phase $g_{(-)}(b)$ into (12) or with a help of modification of the stationary-phase method, for instance, following ref. [19]. In the next section, this case is considered in detail.

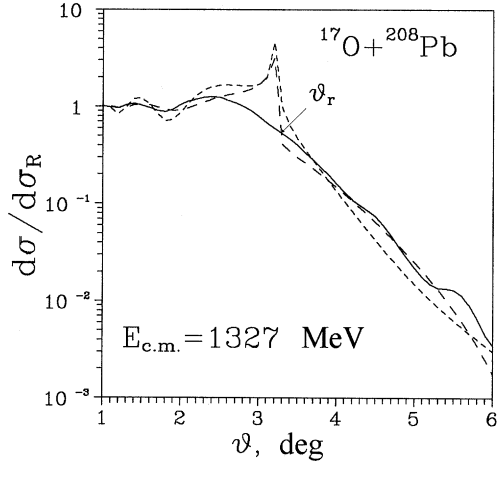

Рис 2: *The ratio of differential cross sections $d\sigma/d\sigma_R$ for reaction $^{17}O + {}^{208}Pb$. The potential parameters are the same as in Fig.1. The solid curve is an exact numerical calculation with $W_0 \neq 0$. Calculation by the stationary-phase method: small-dashed lines are for $W_0 = 0$ (no absorption), dashed curves are for $W_0 \neq 0$ (with absorption).*

The behavior of the amplitude for angles $\vartheta > \vartheta_r$ far from the region of classical scattering can be understood from qualitative considerations by using the same parametrization (16) for the function $q(b)$ employed in the region of classical angles. For $q > q_r$, from (17), we have $\sqrt{q_r - q} = i\sqrt{q - q_r}$. In this case, the only the saddle point b_{s_1} remains physically substantiated that determines the exponential drop of the scattering amplitude $f_{(-)} \sim \exp(-q\ Im(b_{s_1}))$ and the corresponding cross section (see dashed curves in the region of $\vartheta > \vartheta_r$ in Fig. 2). This behavior is also confirmed by numerical calculations (a solid curve) and is observed experimentally.

4 The region of Coulomb rainbow

Let us consider the region of angles around ϑ_r where a broad maximum is experimentally observed in the angular distribution of the scattering that is called the rainbow scattering. It is analogous to the phenomenon of natural rainbow in optics that arises from interference between reflected and refracted rays of light in a drop of water, whose sizes are large as compared to the light wavelength. In our case, it is the interference of two amplitudes connected with two stationary points from the right and left side of b_r, to which one can make correspond two near trajectories passing close by the limiting classical trajectory of motion. So, we consider the scattering mechanism in the region of $\vartheta_r \simeq |V_{max}(r \simeq R_c)|/E$ when the saddle points merge (Fig. 1), and there arises a stationary point of a higher order.

To obtain the scattering amplitude in that region, we expand the function $g_{(-)}$ in a power series around the rainbow point $b \sim b_r$. Since $g''_{(-)}(b_r) = 0$, one should take into account, at least, terms up to the third order. Considering that $g'_{(-)}(b_r) = -q + q_r$ and $g^{(3)}_{(-)}(b_r) = \chi^{(3)}(b_r)$, we have

$$g_{(-)}(b) = -qb_r + \chi(b_r) - (q - q_r)(b - b_r) + \frac{\chi^{(3)}(b_r)}{6}(b - b_r)^3 + ... \qquad (19)$$

In this case, the stationary-phase method for integral (7) gives

$$t_{(-)} = 2\pi \left[\frac{2}{\chi^{(3)}(b_r)}\right]^{1/3} \sqrt{b_r}\, e^{ig_{(-)}(b_r)} Ai(\sigma), \qquad (20)$$

where the Airy function is defined by the formula

$$Ai(\sigma) = \frac{1}{2\pi} \int_{-\infty}^{\infty} e^{i(\sigma z + z^3/3)} dz, \qquad \sigma = (q - q_r)\left[\frac{-2}{\chi^{(3)}(b_r)}\right]^{1/3}. \qquad (21)$$

This is the so-called Airy approximation for rainbow scattering usually employed in diffraction models. Like in the case of the Fresnel diffraction, the rainbow scattering (Coulomb rainbow) is determined by the near amplitude $f_{(-)}$.

Because of a particular behavior of the Airy function on the "lighted side" of the rainbow ($\vartheta < \vartheta_r$) , oscillations of the cross sections are observed, and they rapidly damp when moving away from ϑ_r; on the "shadow side", $\vartheta > \vartheta_r$ the cross section decreases quickly. The maximum of the angular distribution is located on the lighted side and corresponds to the maximum of the Airy function (a wave rainbow) when $\sigma = -1$. The limit angle ϑ_r in this case determines the position of the classical rainbow (a geometrical rainbow).

In Fig. 3, comparison of numerical (solid lines) and analytic calculations is given for the cross section of scattering near the rainbow angle for the case of high energies (Fig. 3a) and low energies (Fig. 3b) and different pairs of interacting nuclei. It is seen

that the computation by the analytic stationary-phase method in the traditional Airy approximation (20) (dashed curves) gives no satisfactory description for the nucleus–nucleus scattering. These curves in both the cases go considerably below the solid curves calculated numerically. When the absorption is included through the change of V_0 by $V_0 + iW_0$, still larger disagreement takes place. A possible reason seems to be that the expansion of the function $g_{(-)}$ in the series up to the third-order terms (19) is not sufficient. In particular, it could be verified that the expansion of $g_{(-)}$ (19) for the scattering of ^{17}O by ^{208}Pb agrees with the function $g_{(-)}$ computed numerically only in the region of $b = b_r \pm 0.5\ fm$, which corresponds to the scattering in a highly narrow angular range. To obtain an adequate description of the nucleus–nucleus scattering around ϑ_r we employed the method applicable when two saddle points of the first order are close to each other [19]. Within this method, the expansion in the exponential is made not in the vicinity of the stationary point of second order, but in the vicinity of a midpoint betweenb_{s_1} and b_{s_2} that, in the limiting case, turns into a point of a higher order.

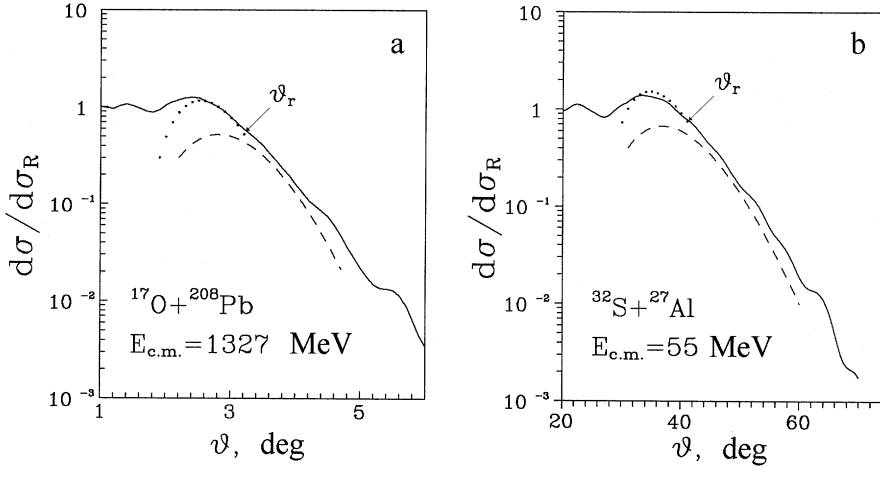

Рис 3: *The ratio $d\sigma/d\sigma_R$ in the region of the rainbow angle. Solid curves are the exact numerical calculation with $W_0 \neq 0$. Calculations by the stationary-phase method: dashed curves are calculated by formula (20); dotted curves are calculations for the case of two neighboring points by formula (22). The potential parameters are listed in Table 1.*

According to the procedure given in [18], the integral (7) can be written in the form

$$t_{(-)} = \pi\sigma^{1/4}\left(h_1\sqrt{b_{s_1}} + h_2\sqrt{b_{s_2}}\right)\, e^{ia_0} Ai(\sigma), \qquad (22)$$

where

$$h_{1,2} = \sqrt{\frac{\mp 2}{g''_{(-)}(b_{s_{1,2}})}}, \qquad a_0 = \frac{1}{2}\big[g_{(-)}(b_{s_1}) + g_{(-)}(b_{s_2})\big], \qquad \sigma = \big[\frac{3}{4}(g_{(-)}(b_{s_1}) - g_{(-)}(b_{s_2}))\big]^{2/3}. \tag{23}$$

When $b_{s_1} \to b_{s_2}$, then $g''_{(-)}(b_{s_{1,2}}) \to 0$. In this limiting case

$$h_1 = h_2 = \Big[\frac{-2}{g^{(3)}_{(-)}(b_r)}\Big]^{1/3}, \qquad b_{s_1} = b_{s_2} = b_r.$$

The saddle point $b_{s_2} \sim b_r$ is expressed by formula (17).

The cross section calculated by (22) is plotted in Fig. 3 by dotted curves. It is seen, that they are in good agreement with the cross section computed numerically on the left of the limiting classical angle ϑ_r including the region of the wave rainbow angles, the maximum of the ratio $d\sigma/d\sigma_R$. As it has been shown, at angles either larger or smaller with respect to the range of rainbow, the cross section can be interpreted as the Fresnel diffraction.

5 The Fraunhofer scattering

Here, we will thoroughly examine the behavior of the elastic scattering cross section at angles $\vartheta > \vartheta_r$, i.e., in the region inaccessible for classical scattering. We saw that the Fresnel picture "works" well in the classically accessible region, and at $\vartheta > \vartheta_r$, it shows a smooth exponential damping, which is natural beyond the scope of classical scattering. However, in this region, the frequently observed experimental patterns are when differential cross sections fall off and oscillate simultaneously that are typical of the Fraunhover diffraction in optics. If use is made of the optical potential with real and imaginary parts,it is possible to explain many nuances of the behavior of cross sections in this region of angles. Theoretically, a new point is that, now, there are stationary points b_{s_n} in the range of integration $Re(b_{s_n}) > 0$ for the near- $f_{(-)}$ and far-side $f_{(+)}$ components of the whole amplitude $f(q)$. They shift into the complex plane of the impact parameter b into the region where poles of the function $u_{SF}(b)$ of the nuclear phase are disposed at $r_p^{\pm}(\epsilon) = \pm R + \epsilon i\pi a(2p-1)$, with p=1,2,3..., $\epsilon = \pm 1$. In ref. [20], an attempt has been made to explicitly find the profile integral with the Fermi function $\int_{-\infty}^{\infty} u_F(\sqrt{b^2+z^2})dz$ in phase (2) through continuing into the complex plane. The answer was given by the sum of residues at poles of the Fermi function $r_p^{\pm} = R \pm i\pi a(2p-1)$, $(p = 1, 2, 3...)$. However, in the limit $b \to 0$, the sum was 0, instead of the correct value $\simeq R$. Therefore, the authors of ref. [20] have proposed the following prescription

$$\chi_N(b) = -kR\frac{V_0 + iW_0}{E}\Big[1 - i\pi\frac{a}{R}\sum_{p=1}^{\infty}\Big(\frac{r_p^+}{\lambda_p^{(+)}} + \frac{r_p^-}{\lambda_p^{(-)}}\Big)\Big], \tag{24}$$

where $\lambda_p^{(\pm)} = \sqrt{(r_p^{\pm})^2 - b^2}$, and the condition $Im\ \lambda_p^{(\pm)} \geq 0$ should hold. Numerical verification shows that this function correctly reproduces the behavior of the profile integral in the complex plane, at least, around the poles nearest to the real axis b. At the same time, expression (24) does not give the accuracy required for the phase χ_N on the real axis in the range of $b > R$, even if several hundred terms are kept in the sum. For further consideration, it should be remembered that, when amplitudes are estimated asymptotically, saddle points are displayed in the region of extremums of the phase. Therefore the amplitudes under consideration are changed sharply in the complex plane just near singularities of the phase, the poles $\chi_N(b)$. A major contribution to the amplitude for $q \gg q_r$ comes from the two poles $r_1^{\pm} = R \pm i\pi a$ nearest to the real axis, and every next pair with $p > 1$ brings a correction by a factor $\exp(-\pi a q)$ lower than the previous one. However, a more accurate result can be achieved if the total contribution of remaining terms with $p \geq 2$ of the sum in (24) is simulated, in the region of $r_1^{\pm}$-poles, by the smooth function $\Delta(b)$ [21] rather than neglecting contributions from the poles with $p \geq 2$, as it was made in [22]. It is just this modified expression, we will use for the nuclear phase

$$\chi_N(b) = -kR\frac{V_0 + iW_0}{E}\Big[1 - i\pi\frac{a}{R}\Big(\frac{r_1^+}{\lambda_1^{(+)}} + \frac{r_1^-}{\lambda_1^{(-)}}\Big) + \frac{\Delta(b)}{2R}\Big], \tag{25}$$

The function $\Delta(b) = \Delta_R(b) + i\Delta_I(b)$ where $b = b_1 + ib_2$ can be found in [21]; for the Coulomb phase, we take, as before, the asymptotic value $\chi_C = 2\eta\ln(kb)$.

In the case when stationary points are looked for in the region of sharp change of the phase, small contributions from the derivatives of smooth functions $\chi_C(b)$ and $\Delta(b)$ can be neglected. Since contributions in the near- and far-side amplitudes are made, correspondingly, to the saddle points lying in the first and forth quadrants of the complex plane b, then, in parentheses of eq.(25), only the first term can be kept for $f_{(+)}$, whereas, for $f_{(-)}$, only the second term (see [21]). In this way, we extended the approach to nucleus–nucleus scattering developed in ref. [22], in which only the pole in the first quadrant was taken into account. Now, the equation for the saddle point takes the form

$$g'_{(\pm)}(b) = \pm q + \bar{\alpha}\frac{r_1^{\pm}\, b}{\left(\lambda_1^{(\pm)}\right)^3} = 0, \tag{26}$$

where

$$\bar{\alpha} = -\pi a k\frac{|W_0| - i|V_0|}{E} = |\alpha|\ e^{i\beta_\alpha}, \tag{27}$$

$$\beta_\alpha = 2\pi - \arcsin\frac{1}{\sqrt{1 + (W_0/V_0)^2}}. \tag{28}$$

Also, the following formulae

$$r_1^{\pm} = R \pm i\pi a = |r^{\pm}|\ e^{i\beta_r^{(\pm)}}, \tag{29}$$

$$\beta_r^{(+)} = \arcsin \frac{\pi a}{\sqrt{\pi^2 a^2 + R^2}} \simeq \frac{\pi a}{R}, \qquad \beta_r^{(-)} = 2\pi - \beta_r^{(+)} \tag{30}$$

are useful. Following the procedure of ref. [22], we look for solutions to eq.(26) around the poles $r_1^{\pm}$ in the form

$$b_s^{(\pm)} = r_1^{\pm} + \delta^{(\pm)}, \tag{31}$$

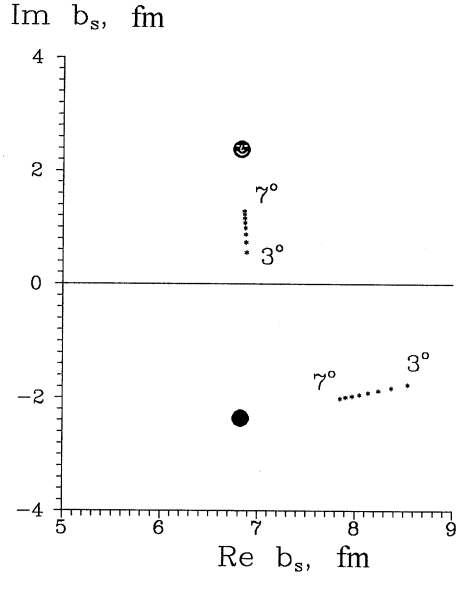

Рис 4: *Motion of saddle points in the complex plane b with growing angle* ϑ $(3° \div 7°)$ *for scattering* $^{17}O + {}^{60}Ni$. *The potential parameters are listed in Table 1. Large circles are poles* $r_1^{\pm} = R \pm i\pi a$; *and asterisks, calculations by approximate formulae (31) and (35).*

With the help of the condition $|\delta^{(\pm)}| \ll |r_1^{\pm}|$, one can reduce equation (26) to an equation of third order for the quantity $\lambda^{(\pm)}$ and find its roots

$$\lambda_n^{(\pm)} = |\lambda|\, e^{i\beta_\lambda^{(\pm)}}, \qquad |\lambda| = \left[\frac{|\alpha||r^{\pm}|^2}{q}\right]^{1/3}, \tag{32}$$

$$\beta_\lambda^{(\pm)} = \frac{\pi}{3}\left[2n + \frac{1}{2} \pm \frac{1}{2}\right] + \frac{1}{3}\beta_\alpha + \frac{2}{3}\beta_r^{(\pm)}, \tag{33}$$

for which $Im\ \lambda_n^{(\pm)} \geq 0$, and the solutions $b_s^{(\pm)}$ are in I and IV quadrants [21]. Using the condition $|\delta^{(\pm)}| \ll |r_1^{\pm}|$, we arrive at

$$\lambda_n^{(\pm)} = \sqrt{(r_1^{\pm} + b_{s_n}^{(\pm)})(r_1^{\pm} - b_{s_n}^{(\pm)})} \simeq \sqrt{-2r_1^{\pm}\delta_n^{(\pm)}}, \tag{34}$$

and then, from eq.(32), we obtain the final expression

$$\delta_n^{(\pm)} = -\frac{1}{2}\frac{|\lambda|^2}{|r_1^{(\pm)}|}\, e^{i\beta_\delta^{(\pm)}}, \qquad \beta_\delta^{(\pm)} = \frac{2}{3}\pi(2n+1) + \frac{2}{3}\beta_\alpha \pm \frac{1}{3}\beta_r^{(+)}. \tag{35}$$

The behavior of saddle points in the complex plane b determined from approximate formulae (31) and (35) is shown in Fig. 4. The sum of the near- and far-side amplitudes calculated with these points determines the Fraunhofer type diffraction scattering. The detail discussion of the latter is done in Sect. 6.

6 Discussion of results. The trajectory distortion

In Fig. 5 for the reactions of elastic scattering of ^{17}O on nuclei ^{208}Pb, ^{120}Sn, ^{90}Zr, ^{60}Ni it is shown that different scattering mechanisms operate in different ranges of the angular distribution. Scattering in the range $\vartheta < \vartheta_r$ (regions I, II) is described by the sum of two terms of the near-side amplitude; and each of them is specified by its own impact parameter b_{s_1} and b_{s_2}. So, there are two trajectories in the range of action of the Coulomb potential and the tail of nuclear potential that provide scattering through the same angle.

At very small angles, the contribution from the nuclear trajectory is negligible because of strong absorption of particles at small b_{s_1}. In this case, scattering is governed by the Coulomb trajectory with a large impact parameter b_{s_2}, and the ratio $d\sigma/d\sigma_R$ is close to unity. When ϑ is increased, the saddle points $q(b_{s_1})$ on the nuclear slope are shifted towards larger periphery of the nuclear potential where absorption is small, and the role of its real part responsible for refraction grows. As a result, the interference picture in the region I of angular distribution gets more pronounced. It is accepted to be associated with the Fresnel diffraction.

A specific feature of the angular distribution in the region II is that there is a limiting scattering angle ϑ_r, near which the classical trajectories are bunched. Just for this reason, one can draw analogy with the optical interference of refracted and once reflected rays of light in a drop of water (rainbow scattering). At $\vartheta < \vartheta_r$, the regions I and II are clearly distinguished, and the point of matching of corresponding cross sections is determined definitely. From Fig. 5 it is seen that the calculations by formula (15), dashed curves, are in good agreement with the exact numerical integration of the initial amplitude (1), solid curves, up to the position of broad maxima of the angular distributions. This is the region I. Then up to the limiting scattering angles (region II), the numerical results are reproduced by formula (22) for rainbow scattering (dotted curves). The position of maxima of the angular distributions corresponds to the maximum of the function $Ai(\sigma)$ in expression (22) when $\sigma = -1$. If at a given angle ϑ we have $\sigma < -1$, then for the amplitude, one should employ expression (12); otherwise, use should be made of formula (22). The long dashed curves calculated by eq. (20) (the akin expression

is frequently employed in diffraction models for the rainbow scattering) are fairly lower than the numerical ones (solid curves). For lighter nuclei at the same collision energy, the maximum of the angular distribution is displaced into the region of smaller angles; this corresponds to narrowing of the classical scattering region.

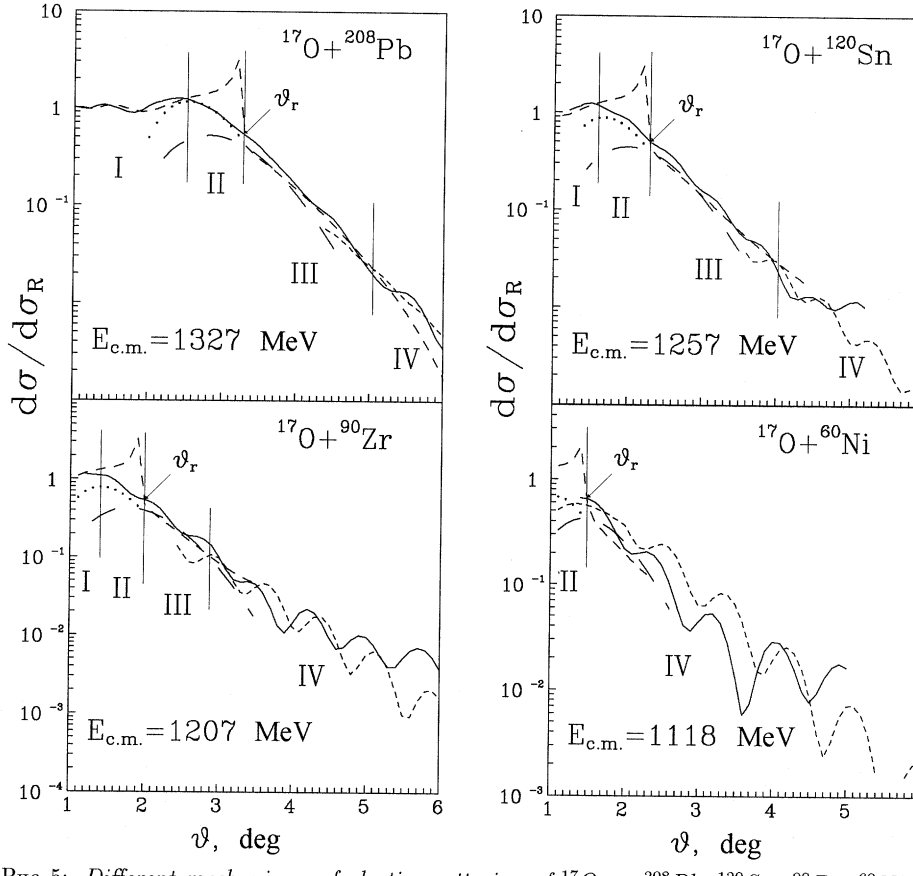

Рис 5: *Different mechanisms of elastic scattering of ^{17}O on ^{208}Pb, ^{120}Sn, ^{90}Zr, ^{60}Ni. I is the Fresnel diffraction; II, the rainbow scattering; III, the region of the near-side amplitude; IV, the Fraunhofer scattering. The solid curves are the numerical calculations; the dashed curves are calculated by eq.(14); the long-dashed curves, by eq.(20); the dotted curves, by eq.(22), the small-dashed curves, see sect. 5. The parameters are in Table 1.*

In the quantum scattering region ($\vartheta > \vartheta_r$), the stationary points are displaced in the complex plane. Typically, the experimental cross-section data for $\vartheta > \vartheta_r$ drop exponentially without oscillations (region III) and/or with oscillations (region IV). In the first case, a major contribution to the amplitude comes from the near amplitude with one complex stationary point b_{s_1} (eq. (17)) when $q > q_r$ (dashed lines). In region IV, the

cross section oscillates because of addition of the near and far amplitudes (small-dotted lines) (Fraunhofer scattering). When calculating these amplitudes, the saddle points were computed on the complex plane provided the absorption is taken into account. In contradistinction to the classical region, the choice of the point of matching is here arbitrary. We have found that solutions corresponding to regions III and IV are matched at the point of their intersection nearest to ϑ_r from the right side. It is to be noted that, with diminishing the ratio of the Coulomb barrier to the collision energy V_B/E, scattering in the quantum region assumes a more clear Fraunhofer character.

Consider the problem of the Coulomb distortion of a trajectory. Under the action of a strong Coulomb repulsion, the trajectory of heavy ions deviates strongly from a straight line, which influences the behavior of the cross section noticeably. To take this distortion into account [24], if, in the nuclear phase (2), we change the impact parameter b to the corresponding distance of closest approach in the Coulomb field $Z_1 Z_2 e^2/r$:

$$\chi_N(b) \to \chi_N(b_c), \qquad b_c = a_c + \sqrt{b^2 + a_c^2}, \tag{36}$$

where $a_c = \eta/k$ is a half-distance of closest approach in a head-on collision. It is obvious that the change $b \to b_c$ complicates the shape of derivatives of χ_N with respect to b, however, this produces an explicit expression for the limiting classical momentum transfer $q_{max} \equiv q_r$ and stationary points.

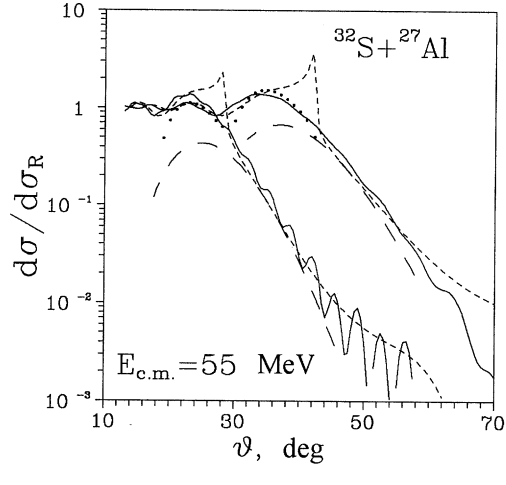

Рис 6: *Influence of the Coulomb distortion of a trajectory for the scattering of* ^{32}S *on* ^{27}Al *at* $E_{c.m.} = 55\ MeV$. *The left curves are obtained without the distortion* $a_c = 0$); *the right ones, with the distortion* $a_c \neq 0$. *All the curves are calculated like those in Fig.5.*

In Fig. 6, we compare numerical (solid lines) and analytic calculations (dashed and dotted lines) of the ratio $d\sigma/d\sigma_R$ for elastic scattering of ^{32}S on ^{27}Al at $E_{c.m.} = 55\ MeV$.

Curves without Coulomb distortion ($a_c = 0$) are shown in the left part of the figure; whereas those with the Coulomb distortion ($a_c \neq 0$), in the right part. It is seen that the distortion strongly shifts the picture of angular distribution; and analytic calculations are in good agreement with numerical ones. As mentioned before, the cross section is highly sensitive to the position of the maximum of the deviation function. Therefore, it is important to exactly determine the quantities q_r and b_r with taking account of the Coulomb distortion in the initial phase even if a_c is small.

In considering the Fraunhofer scattering we saw that the stationary points b_s are complex. In this case, the distortion was taken into account through the change of b_s in the phase in the final expression for the amplitude as follows:

$$b_s \to \tilde{b}_s = a_c + \sqrt{b_s^2 + a_c^2}. \tag{37}$$

Our calculations gave evidence that this change should be introduce when $V_B > 0.04E$.

Table 1.

The potential parameters for reactions of elastic scattering of ^{17}O on nuclei ^{208}Pb, ^{120}Sn, ^{90}Zr, ^{60}Ni [25] and scattering of ^{32}S on ^{27}Al [26].

	$E_{c.m.}$, MeV	V_0, MeV	W_0, MeV	R, fm	a, fm	R_C, fm
$^{17}O + ^{208}Pb$	1327	50	47.1	9.286	0.727	10.196
$^{17}O + ^{120}Sn$	1257	50	45.0	8.171	0.706	9.0
$^{17}O + ^{90}Zr$	1207	50	37.1	7.666	0.697	8.463
$^{17}O + ^{60}Ni$	1118	50	39.5	6.823	0.754	7.783
$^{32}S + ^{27}Al$	55	100	48.76	7.428	0.5	7.428

In Fig. 7, the analytic calculations are presented matched at points of intersection of curves for different scattering mechanisms. The curves were calculated with the Coulomb distortion taken into account. It is seen that the analytic methods developed here reproduce the main features of experimental data [25] in all the regions of the scattering angles. Minor deviations of theoretical curves from the experimental points show that the nuclear forces should be also included in distortion of the trajectory of motion, especially in the Fraunhofer diffraction region where the amplitude is considered on the complex plane.

On the whole, we can conclude that the Glauber–Sitenko approximation is applicable for considering nucleus–nucleus collisions at energies of an order of 10–100 MeV/nucleon.

The range of applicability with respect to the scattering angles is expanded at the expense of the Coulomb shift of the trajectory of motion of an incident ion by $\vartheta_c \simeq V_{max}(r \sim R)/E$.

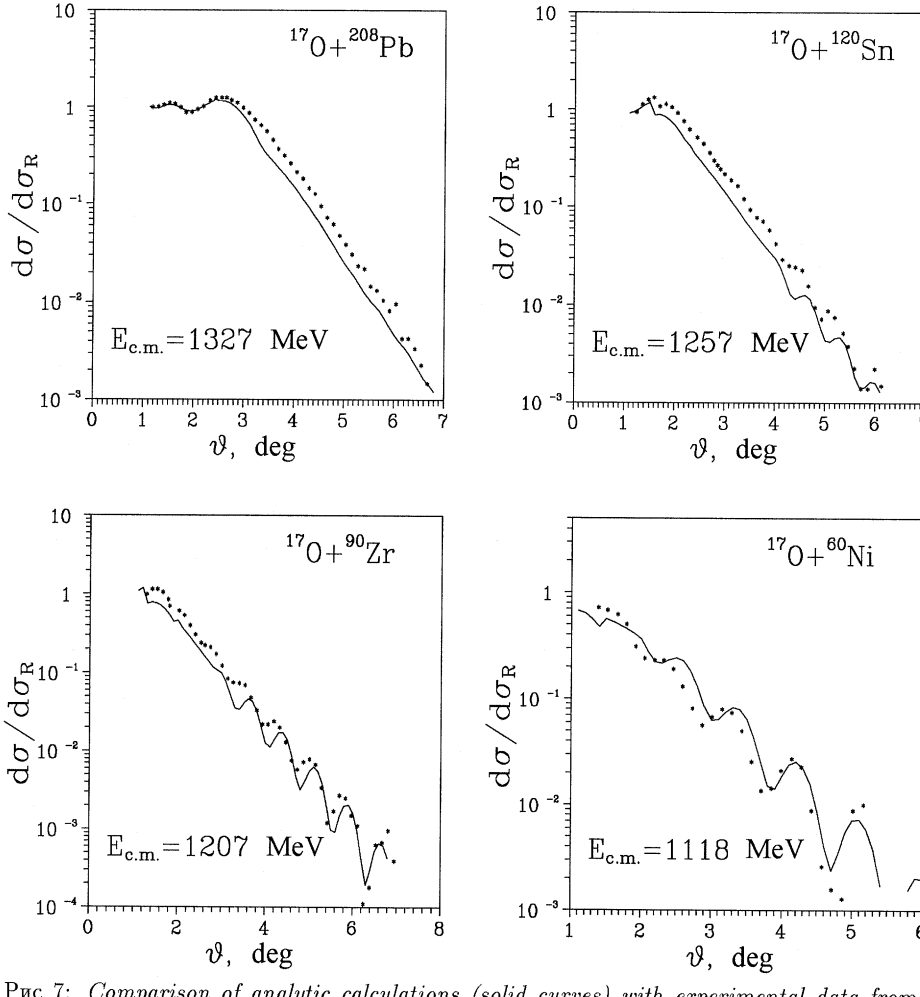

Рис 7: *Comparison of analytic calculations (solid curves) with experimental data from ref.[25]. The different scattering mechanisms are matched as shown in Fig.5.*

In this way, there appear conditionally separated regions of angles of the classical $\vartheta < \vartheta_c$ and quantum scattering $\vartheta_c < \vartheta < \vartheta_c + \sqrt{2/kR}$ with their proper peculiarities of interference and diffraction. The use of the explicit form of the eikonal phase for the extended optical Woods–Saxon potential allowed one to develop the asymptotic methods of calculating the eikonal amplitudes in this energy region and to describe the nucleus–nucleus scattering in terms of diffraction models. It turns out that the construction of

responsible analytic methods and the calculations of scattering amplitudes are rather sensitive to the behavior of the potential in a rather narrow region of its periphery. The consideration of these peculiarities makes it possible to understand the scattering mechanism qualitatively and to describe main features of experimental differential cross sections quantitatively.

The authors (V.K.L. and Yu.V.Ch.) are thankful to the Russian Foundation for Basic Research for support, grant 00-15-9673.

Appendix A. Coefficients of the logarithmic parabola in terms of the input parameters of the reaction

According to (13), the deviation function is given by

$$q = \chi'_N + \chi'_C. \qquad (\Pi.1)$$

Inserting χ_N (11) and $\chi_C = 2\eta \ln(kb)$ into this expression, we obtain

$$q = \frac{2\eta}{b} + \gamma_N \; 2RP(1,C)u'_{SF}(b), \qquad (\Pi.2)$$

It is impossible to derive the explicit dependence $b = b(q)$ for stationary points from this equation. Therefore, in the region of the maximum of the deviation function ($q_{max} = q_r = q(b_r)$), we approximate the right-hand side of (П.2) by the logarithmic parabola $q = q_r - \rho[\ln\{(b - b_1)/(b_r - b_1)\}]^2$ (16), and for it, the stationary paints are determined explicitly (17). However, for this approximation, one should accurately determine the position of the maximum, i.e.q_r end b_r,- main parameters of the logarithmic parabola. At the point b_r the derivative of (П.2) is equal to zero, and we arrive at the equation

$$-\frac{2\eta}{(b_r/a)^2} + \gamma_N \; 2RP(1,C)u''_{SF}(b) = 0. \qquad (\Pi.3)$$

The most suitable method for its explicit solution is the reduce it to a third-order equation. The latter has at least one real solution that determines the position of the maximum. In the case of three real roots, the sought b_r is the one nearest to the radius of the nuclear potential R.

To determine the coefficients of the polynomial of third degree that passes through zero of expression (П.3), we take four points x_n, $(n = 0, 1, 2, 3)$ on the tail of the nuclear potential as follows [4]

$$u_F(x_0) = 0.005, \quad u_F(x_1) = 0.01, \quad u_F(x_2) = 0.02, \quad u_F(x_3) = 0.05. \qquad (\Pi.4)$$

[4]For simplicity, we use here u_F instead of u_{SF} that coincide at real $b > 0$.

Then they can easily be expressed in terms of the potential geometric parameters

$$x_0 = R + a\ln(199), \qquad x_1 = R + a\ln(99),$$
$$x_2 = R + a\ln(49), \qquad x_3 = R + a\ln(19). \tag{П.5}$$

Using these points, we construct the interpolation Newton polynomial [27]

$$\phi(b) = \phi(x_0) + (b - x_0)\ \phi(x_0, x_1) + (b - x_0)(b - x_1)\ \phi(x_0, x_1, x_2)$$
$$+(b - x_0)(b - x_1)(b - x_2)\ \phi(x_0, x_1, x_2, x_3), \tag{П.6}$$

where $\phi(x_n)$ are the values of expression (П.3) at points x_n, and $\phi(x_0, ..., x_n)$ are divided differences of an n-th order of the form:

$$\phi(x_0, x_1) = \frac{\phi(x_0) - \phi(x_1)}{x_0 - x_1}, \qquad \phi(x_0, x_1, x_2) = \frac{\phi(x_0, x_1) - \phi(x_1, x_2)}{x_0 - x_2},$$

$$\phi(x_0, x_1, x_2, x_3) = \frac{\phi(x_0, x_1, x_2) - \phi(x_1, x_2, x_3)}{x_0 - x_3}.$$

Removing brackets in (П.6) and collecting coefficients of the same degrees of b, we arrive at an equation of third order, whose real solution determines b_r, and q_r is obtained by direct substitution of b_r into (П.2). To determine b_1, we approximate the function $q(b)$ by a parabola with the vertex at point (b_r, q_r), i.e. $q(b) = q_r - A(b - b_r)^2$. Requiring the parabola to pass through a point (for instance, x_3) on the left branch of $q(b)$, we obtain the coefficient A; then, $b_1 = b_r - \sqrt{q_r/A}$. The coefficient ρ is determined from the condition of coincidence of the logarithmic parabola with the function $q(b)$ (П.2) at an arbitrary point from the interval $[b_1; b_r]$; we took it equal to $(b_1 + b_r)/2$.

The method proposed did not take account of the effect of deviation of a trajectory under the action of the Coulomb field. This can be done by using the same conditions (П.4) for the function $u_F(\tilde{x})$ where $\tilde{x} = a_c + \sqrt{x^2 + a_c^2}$. Note that the change of x by $\tilde{x}$ in (П.1)leads to more cumbersome expressions for derivatives in (П.2) and (П.3), however, does not change the above scheme of determination of b_r, q_r, b_1 end ρ.

Список литературы

[1] M.S. Hussein, K.W. McVoy, Prog. Part. Nucl. Phys. **12**, 103 (1984).

[2] W.E. Frahn, *Diffractive Processes in Nuclear Physics* (Clarendon Press, Oxford, 1985).

[3] E.V. Inopin, A.V. Shebeko, *Diffraction Interaction of Hadrons with Nuclei* (Naukova dumka, Kiev, 1987) p.154.

[4] A.I. Akhiezer, Yu. A. Berezhnoy, V.V. Pilipenko, Phys. of Elem. Part.& Nucl. Struct., **31**, 458 (2000).

[5] G.R. Satchler, W.G. Love, Phys. Rep. **55**, 183 (1979).

[6] Dao Tien Khoa, O.M. Knyazykov, Phys. of Elem. Part.& Nucl. Struct., **21**, 1456 (1990).

[7] Dao Tien Khoa, G.R. Satchler, W. von Oertzen, Phys. Lett. B **358**, 14 (1995).

[8] O.M. Knyaszykov, I.N. Kuhtina, S.A. Fayans, Phys. of Elem. Part.& Nucl. Struct.,**28**, 1061 (1997).

[9] R.J. Glauber, *Lectures in Theoretical Physics* (Interscience, New York, 315, 1959).

[10] A.G. Sitenko, Ukr. Phys. J. **4**, 152 (1959).

[11] V.K. Lukyanov, E.V. Zemlyanaya, J. Phys. G **26**, 357 (2000).

[12] G. Faldt, Phys. Rev. D **2**, 846 (1970).

[13] O.D. Dalkarov, V.A. Karmanov, Nucl. Phys. A **445**, 579 (1985).

[14] P.J.Karol, Phys. Rev. C **11**, 1203 (1975).

[15] M. Grypeos, C. Koutroulos, V. Lukyanov, V. Shebeko, J.Phys.G, **24**, 1913 (1998).

[16] V.K. Lukyanov, Phys. Atomic Nucl. **58**, 1848 (1995) (transl. from russ.Yad.Fiz.**58**, 1955 (1995)).

[17] N. Rowley, C. Marty, Nucl. Phys. A **266**, 494 (1976).

[18] K.W. Ford, J.A. Wheeler, Ann. Phys. **7(3)**, 287 (1959);

[19] L.B. Felsen, N. Marcuvitz, *Radiation and Scattering of Waves* (Prentice-Hall, Inc., Englewood Cliffs, New Jerscy 1973) V.1, Ch.4.

[20] J.R. Shepard and E. Rost // Phys. Rev. C, v.25, 1982, p.2660.

[21] V.K. Lukyanov, V.P. Permyakov, Yu.V. Chubov, Bull. of Russ. Acad. Sc., Physics, **63**, 54 (1999).

[22] R.D. Amado, J.P. Dedonder, F. Lenz, Phys. Rev. C **21**, 647 (1980).

[23] A.V. Embulaev, E.V. Zemlyanaya, V.K. Lukyanov, V.P. Permyakov, Yu.V. Chubov, Bull. of Russ. Acad. Sc., Physics, **62**, 2136 (1998).

[24] A. Vitturi, F. Zardi, Phys.Rev. C **38**, 2086 (1988).

[25] R. Liguori Neto et al., Nucl. Phys. A **560**, 733 (1993).

[26] D.J. Garrett et al., Phys. Rev. C **12**, 489 (1975).

[27] N.N. Kalitkin, *Numerical Methods* (Science, Moscow, 1978).

Received by Publishing Department
on April 18, 2001.

Лукьянов В.К., Пермяков В.П., Чубов Ю.В.
Е4-2001-75

Описание упругого рассеяния тяжелых ионов
в рамках подхода Глаубера–Ситенко

В рамках высокоэнергетического приближения Глаубера–Ситенко получены аналитические выражения для амплитуд упругого ядро-ядерного рассеяния, соответствующие различным режимам столкновения. При этом используется протяженный оптический потенциал типа Вудса–Саксона и учтено отклонение траекторий сильным кулоновским полем. Сравнение аналитических расчетов сечений с численными результатами и экспериментальными данными показывает, что подход можно успешно применять в области энергий 10–100 МэВ/нуклон. Показано, что при заданном потенциале можно найти угловые интервалы, где преимущественно проявляется определенная картина рассеяния, как, например, классическое или радужное рассеяние, дифракция Френеля или Фраунгофера.

Работа выполнена в Лаборатории теоретической физики им. Н.Н.Боголюбова ОИЯИ.

Препринт Объединенного института ядерных исследований. Дубна, 2001

Lukyanov V.K., Permyakov V.P., Chubov Yu.V.
E4-2001-75

Description of Elastic Scattering of Heavy Ions
in the Glauber–Sitenko Approach

In the framework of the Glauber–Sitenko approach, analytic expressions are derived for the amplitudes of elastic nucleus-nucleus scattering corresponding to different regimes of collision. An extended optical potential of the Woods–Saxon type is employed in calculations, and the deviation of trajectories by a strong Coulomb field is taken into account. Comparison of the analytic evaluations of cross sections with the numerical results and experimental data show that the approach can be used in the energy region from 10 to 100 MeV/nucleon. In this way, at a given potential, one can find angular ranges where a definite picture of scattering like, for instance, the classical or rainbow scattering, the Fraunhofer or Fresnel diffraction takes place.

The investigation has been performed at the Bogoliubov Laboratory of Theoretical Physics, JINR.

Preprint of the Joint Institute for Nuclear Research. Dubna, 2001

Макет Т.Е.Попеко

Подписано в печать 09.06.2001
Формат 60 × 90/16. Офсетная печать. Уч.-изд. листов 2,28
Тираж 360. Заказ 52705. Цена 2 р. 70 к.

Издательский отдел Объединенного института ядерных исследований
Дубна Московской области